Available online at www.sciencedirect.com

ScienceDirect

Energy Procedia 75 (2015) 1575 – 1582

Energy Procedia

The 7th International Conference on Applied Energy – ICAE2015

Thermal stability analysis of perfluorohexane

Silvia Lasala[a,*], Costante Invernizzi[b], Paolo Iora[b], Paolo Chiesa[a], Ennio Macchi[a]

[a] *Politecnico di Milano, Department of Energy, Via Lambruschini 4, 20156 Milano, Italy*
[b] *University of Brescia, Department of Mechanical and Industrial Engineering, Via Branze 38, 25123 Brescia, Italy*

Abstract

The thermal stability analysis of perfluorohexane (C_6F_{14}) is presented in this paper as a preliminary evaluation of the potential application of the binary mixture CO_2 – C_6F_{14} as innovative working fluid for transcritical-CO_2 power cycles. After presenting a description of the experimental apparatus, saturation pressure models are compared and calibrated over measurements of the virgin fluid (C_6F_{14}). Moreover, the methodology applied to attest the occurrence of a thermal decomposition is described. Finally, the paper presents a thermodynamic analysis of the measurements obtained from the partially decomposed system, performed to investigate the nature of the partial thermal decomposition process.

Peer-review under responsibility of Applied Energy Innovation Institute

Keywords: Perfluorohexane; Transcritical cycle; Thermal stability; Thermodynamics

1. Introduction

Supercritical carbon dioxide Brayton cycles have been thoroughly studied and applied since the 1950s for exploiting high–grade heat sources. In recent years, researchers have attested the potentiality of carbon dioxide as a promising working fluid of transcritical power cycles designed to exploit both low-grade heat sources (< 250 °C) and waste heat [1]. However, the low critical temperature of CO_2 (~ 30°C) entails the need for a cycle cooling source being at less than 15°C, not always available.

A more flexible application of CO_2 condensation cycles would require the increase of the critical temperature (40 – 50°C) of pure CO_2 by adding a small amount of a high-critical temperature component. In particular, the latter should be highly soluble in CO_2 and, focussing on binary mixtures composed of a CO_2 content higher than 95%$_{mol}$, its critical temperature has to be sufficiently high, so that the addition of a small amount of this component (< 5%$_{mol}$) leads to mixtures having critical temperatures of 40 – 50 °C. Moreover, the mixture needs to be thermally stable at the highest operating temperature of the power cycle. Finally, the selection of the second component should take into account the need of utilizing non-toxic,

* Corresponding author. Tel.: +39-02-2399-3935
E-mail address: silvia.lasala@polimi.it.

Peer-review under responsibility of Applied Energy Innovation Institute
doi:10.1016/j.egypro.2015.07.358

non-flammable and environmental friendly working fluids.

In view of these considerations, one possible candidate for the mixture is perfluorohexane (C_6F_{14}), given its high stability and solubility in CO_2 [2-4]. Perfluorohexane is characterized by T_c = 449K and p_c = 19bar. Based on calculations carried out with Patel-Teja equation of state [5], the CO_2-C_6F_{14} mixture with a 1–2%$_{mol}$ of C_6F_{14} has T_c = 40-50 °C. However, due to the high molecular mass of C_6F_{14} (338 kg/kmol) and to its considerable GWP (GWP_{20y} = 6600, GWP_{100y} = 9300), a CO_2-C_6F_{14} mixture with a 2%$_{mol}$ of C_6F_{14} corresponds to a C_6F_{14} mass fraction of 14%, thus resulting in GWP_{20y} ~ 895 and GWP_{100y} ~ 1260. As indicated by IPCC [6], those have been estimated by summing the GWP of both CO_2 and C_6F_{14}, weighted relative to their mass fraction. Notably, the obtained GWP_{20y} is lower than GWP of refrigerants currently used in low-grade heat sources ORC. Finally, the resulting mixture is non-toxic and non-flammable. However, no information are presently available on the thermal stability of such a mixture. Before setting up an experimental campaign to analyse the thermal stability of the system CO_2-C_6F_{14}, this paper presents a preliminary study of thermal stability of pure C_6F_{14}. Arnold et al. [7] have previously attested thermal decompositions of C_6F_{14} occurring within 200°C and 450°C, depending on the atmosphere type (inert or oxidizing) and on the eventual exposure to catalyst. However, there are no published data on thermal stability of the fluid in evacuated environments.

In this study, after detailing the experimental apparatus and the applied procedure, measurements and models of saturation pressures of the virgin C_6F_{14} are presented. Afterwards, a quantitative analysis of thermal stress test results is reported. The last section of the paper treats the application of thermodynamics for the investigation of which partial decomposition process could have led to the deviation of the thermodynamic properties of the decomposed fluid.

Nomenclature

Symbols

G	Generic property
N	Number of data points
p	Pressure
T	Temperature
u	Uncertainty
x	Liquid molar fraction
y	Vapour molar fraction

Subscripts

0	Property of the virgin fluid
c	Critical property
i (or *k*)	i-th property (or k-th interval)
mol	Molar property
Ny	Number N of years
ref	Reference value
s	Property relative to thermal stress conditions
sat	Saturation property
T	Property relative to temperature *T*
w	Mass property

Acronyms

GWP	Global Warming Potential
MRD	Mean Relative Deviation $MRD = 1/N \sum_{i=1}^{N} \left\| G_i^{exp} - G_i^{calc} \right\| / G_i^{exp}$
MSE	Mean Squared Error $MSE = 1/N \sum_{i=1}^{N} \left(G_i^{exp} - G_i^{calc} \right)^2$
NIST	National Institute of Standards and Technology
ODP	Ozone Depletion Potential
RMSE	Root Mean Squared Error $RMSE = \sqrt{MSE}$

Accents

~	Functional form
–	Vector of elements

Superscripts

calc	Calculated property
exp	Experimental property
Ti	Property measured at i-th temperature

2. Experimental method

The applied methodology is based on the detection and analysis of deviations in saturation pressure curves acquired after subjecting the fluid to thermal stress tests. In the followings, the main features of the experimental apparatus and procedure are presented in brief, since a detailed description has already been presented by Pasetti et al. in [8].

The apparatus is composed of two main sections: (i) a stainless steel measurement setup of 164 cm^3, where the fluid is loaded, tested and characterized through temperature and pressure measurements; (ii) two temperature controlled environments that consist of, respectively, a thermostatic bath for vapour pressure measurements and a muffle furnace for isothermal stress tests. In particular, the measurement setup is composed of (i) a cylinder containing the sample fluid to be tested, (ii) a type K thermocouple for fluid temperature measurements, (iii) three pressure transducers with the relative maximum operating pressures of 1 bar, 10 bar and 50 bar. Uncertainties of measured T and p measurements are, respectively, 1.04 °C, 1.15 mbar, 11.52 mbar and 57.63 mbar.

Perfluorohexane ($CF_3(CF_2)_4CF_3$, CAS: 355-42-0) has been supplied by Alfa Aesar at a purity level higher than 98%. The mass of the sample fluid is defined on the basis of the requirement of maintaining the system pressure lower than the safety value of 50 bar. In this case, a mass of 66g of C_6F_{14} has been loaded in the cylinder and degassed by repeated vacuum aspirations at about -30 °C. Afterwards, the vapor pressure profile of the virgin fluid has been measured in the temperature range of -30 – 90°C. The vessel was then subjected to the first thermal stress test, maintaining the fluid at 200°C for 80 hours. After-stress-treatment saturation pressures were measured between -20 and 30 °C. The latter process of saturation pressure measurements was performed after each successive thermal stress tests performed at 250, 300, 400 and 450 °C.

3. Saturation pressure measurements

As introduced in the previous paragraph, the saturation pressure profile of the virgin fluid needs to be defined as function of temperature because it represents the reference for attesting the deviation that may occur as consequence of the thermal stress test. Saturation P-T data of the virgin fluid obtained during this campaign (see Table 1) are in agreement with both experimental data obtained by [9-13] and predictions of the model proposed by Wagner in [14,15], used as reference by NIST. Model parameters and fluid critical properties have been selected from NIST database (see Table 2).

As shown in par. 4 and 5, the thermal stability analysis is performed by analysing a reduced amount of saturation P-T data measured after each thermal stress. Thus, another accurate model is required, being characterised by less parameters than those present in the Wagner model. To this end, the Antoine model [16] has been selected and calibrated over saturation measurements presented in Table 1. Table 2 reports the Antoine coefficients regressed in this work by minimizing the global RMSE between model prediction and experimental data included in the range -19,96 °C – 30,04 °C. It was preferred not to consider experimental saturation pressures measured at temperatures higher than 30,04°C (see Table 1) in order to guarantee higher accuracies of the model at low temperature, where deviations of saturation pressures enable the detection of a thermal decomposition process. The accuracies of the two models have been evaluated by calculating and comparing the MRD% in the range -19,96 °C–30,04 °C. As expected, the accuracy of the Wagner model, MRD%=1.7, is higher than the one of the Antoine model, MRD%=3.9. However, considering the high uncertainty on experimental temperature measurements (±1.04°C), the inaccuracy introduced by the Antoine model can be accepted.

Table 1. p_{sat}-T measured in this work†.

T [°C]	$p_{sat,0}^{exp}$[kPa]	T [°C]	$p_{sat,0}^{exp}$ [kPa]
-19.96	2.461	20.09	23.933
-10.05	4.871	30.02	35.820
-9.88	4.871	30.04	36.132
-0.02	8.768	70.67	154.739
10.03	14.726	90.03	269.59

Table 2. C_6F_{14} parameters for Wagner and Antoine models.

Author	*Wagner [10,11]*						*Antoine [12]*		
Equation	$\ln(p_{sat}/p_c) = (A\cdot\tau+B\cdot\tau^{1.5}+C\cdot\tau^{2.5}+D\cdot\tau^{5})/(1-\tau)$ with $\tau = 1- T/T_c$, p /bar, T /K						$\log_{10}(p_{sat})=A-B/(C+T)$ p /kPa, T /K		
Parameters	A	B	C	D	T_c /K	p_c /bar	A	B	C
	-8.969	3.411	-5.516	-2.739	451.1	18.783	7.14	1691.29	0.00
Interp.range	T = -86.08 °C–177.95 °C						T = -19.96 °C–30.04 °C		

4. Results of thermal stress tests

This paragraph presents a preliminary analysis of the experimental data collected during both thermal stress tests and saturation pressure measurements.

In general, if no decompositions occur during a thermal stress test, no variation in the measured pressure should be observed. This is the case of thermal stress tests carried out at T_s = 200, 250, 300 and 350 °C, as shown in Table 3a. On the contrary at T_s = 400 °C, pressure P_{Ts} increases up to the 0,98% of its initial value, $P_{Ts,0}$, while the maximum deviation of stress temperature is 0.11% of $T_{s,0}$. This deviations can be considered indicative of a partial thermal decomposition process.

The pressure increase observed while testing at T_s = 450.7 °C is much more severe (see Figure 1a). In fact, despite the observed reduction of stress temperature, pressure increases from the initial value of 45.26 bar to 48.12 bar. Moreover, Figure 1b shows, for each thermal stress test, 180 averaged experimental points (T_s, p_{Ts}). Here, it can be observed that, differently from the preceding five tests, at T_s = 450 °C there is not a univocal value for pressure p_{Ts}. Concluding, both Figures 1a and 1b show the occurrence of a radical change of thermodynamic properties at 450°C, likely due to modifications arisen in the fluid molecular structure and, thus, in its global composition.

Moreover, saturation pressure curves measured after each thermal stress test performed between 200 and 400°C are compared with those predicted by the Antoine equation initially calibrated over virgin fluid data (see par.3). All these measurements are reported in Table 3b. More specifically, the application of this Antoine equation leads to determine saturation pressures of the virgin C_6F_{14}, p_{sat}^{calc}, as a function of experimental temperatures obtained while measuring after-stress-treatment saturation pressures, $p_{sat,Ts}^{exp}$. Thus, after each thermal stress test at T_s, the overall MSE_{Ts} is determined for the after-stress-treatment saturation pressure curve, accounting for each of the N temperatures, T_i, at which the saturation pressure has been measured: $MSE_{T_s} = N^{-1}\cdot\sum_{i=1}^{N}\left(\left|p_{sat,Ts}^{exp,T_i} - \tilde{p}_{sat}^{calc}(T_i)\right|\right)^2$, with $\tilde{p}_{sat}^{calc}(T_i) = 10^{A-B/(C+T_i)}$ and A, B, C reported in Table 2. For each *i-th* thermal stress temperature $T_{s,i}$, $MSE_{T_{s,i}}$ is compared with a maximum acceptable value of MSE considered as reference, $max(MSE_{Ts})$. In particular, the latter is determined by summing: (i) the mean squared error, MSE_{ref}, evaluated between the experimental saturation pressures of the virgin fluid $p_{sat,0}^{exp,T_i}$ (see Table 1) and predictions, $\tilde{p}_{sat}^{calc}(T_i)$, of the Antoine equation initially calibrated over such saturation pressures: $MSE_{ref} = N^{-1}\cdot\sum_{i=1}^{N}\left(\left|p_{sat,0}^{exp,T_i} - \tilde{p}_{sat}^{calc}(T_i)\right|\right)^2$; (ii) MSE_{ref} uncertainty, $u(MSE_{ref})$, given by the propagation of the uncertainties of T and p measurements, respectively, $u(T^{exp})$ = 1.04 °C and $u(p^{exp})$ = 0.115 kPa:

$$u(MSE_{ref}) = \sqrt{\left(\frac{\partial MSE}{\partial T^{exp}}\right)^2 u^2(T^{exp}) + \left(\frac{\partial MSE}{\partial p^{exp}}\right)^2 u^2(p^{exp})} \quad (1)$$

† Temperature and pressure uncertainties, relative to the T and p ranges reported in table, are ±1.04°C and ±0.115kPa.

where, noting that $\tilde{p}_{sat}^{calc}(T^{exp}) = 10^{A-B/(C+T^{exp})}$,

- $\frac{\partial MSE}{\partial T^{exp}} = N^{-1}\sum_{i=1}^{N}\left(ln10^{2B(C+T_i^{exp})^{-2}}10^{A-B\cdot(C+T_i^{exp})^{-1}}\left|P_{exp}-10^{A-(C+T_i^{exp})^{-1}}\right|\right)$
- $\frac{\partial MSE}{\partial p^{exp}} = 2N^{-1}\sum_{i=1}^{N}\left|p_{sat}^{exp,T_i^{exp}}-\tilde{p}_{sat}^{calc}(T_i^{exp})\right|$

In this case, since the Antoine equation was calibrated by minimizing the RMSE, MSE_{ref} is much smaller than its uncertainty. Hence, it is more meaningful to consider $max(MSE_{Ts}) = u(MSE_{ref})$. In particular, $max(MSE_{Ts}) = 89kPa^2$ and each $MSE_{T_{s,i}}$ is reported in Table 3a. Those have been determined considering N=6 saturation pressures in the range -20 – 35 °C. As observed from the previously detected pressure deviations, the fact that $MSE_{Ts=400°C} > max(MSE_{Ts})$ confirms the anomalous increment of pressure observed during the thermal stability test.

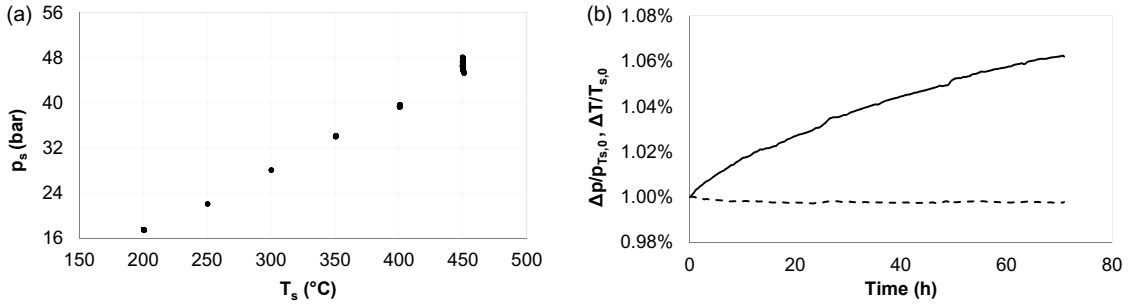

Fig. 1. (a) P_{Ts}–T_s plot of measurements obtained during each thermal stress test; (b) Percentage P and T average relative deviations ($\Delta P = P_{Ts} - P_{Ts,0}$ (—) and $\Delta T = T_s - T_{s,0}$ (- -)) during stress test at $T_s \sim 450°C$, with reference to acquired initial value $P_{Ts,0}$ and $T_{s,0}$.

Table 3. (a) After-stress-treatment measured saturation pressures. (b) Pressure and temperature absolute deviations during each thermal stress test and saturation pressure Mean Squared Errors, MSE_{Ts}

(a)

$T_{s,0}$ [°C]	$P_{Ts,0}$ [bar]	$(T_s-T_{s,0})/T_{s,0}$ max	$(T_s-T_{s,0})/T_{s,0}$ min	$(P_{Ts}-P_{Ts,0})/P_{Ts,0}$ max	$(P_{Ts}-P_{Ts,0})/P_{Ts,0}$ min	MSE_{Ts}
200.5	17.49	0.02%	-0.56%	0.03%	-0.72%	0.2
250.4	22.07	0.07%	-0.28%	0.17%	-0.54%	2.5
300.2	28.08	0.05%	-0.92%	0.07%	-1.16%	5.8
350.0	34.05	0.30%	-0.01%	0.40%	-0.01%	8.2
400.7	**39.27**	**0.11%**	**-0.07%**	**0.98%**	**-0.01%**	**354.5**
450.7	**45.26**	**0.06%**	**-0.26%**	**6.32%**	**-0.01%**	**-**

(b)

Ts=200°C		*Ts=250°C*		*Ts=300°C*		*Ts=350°C*		***Ts=400°C***	
T [°C]	P_{sat,T_s}^{exp} [kPa]	T [°C]	P_{sat,T_s}^{exp} [kPa]	T [°C]	P_{sat,T_s}^{exp} [kPa]	T [°C]	P_{sat,T_s}^{exp} [kPa]	T [°C]	P_{sat,T_s}^{exp} [kPa]
-19.93	2.89	-19.92	3.95	-19.97	4.89	-19.89	4.97	-19.92	**5.43**
-9.94	5.22	-4.99	8.00	-10.06	7.22	-9.96	7.46	-9.96	**8.26**
0.07	9.08	5.03	12.96	-0.01	11.17	0.01	11.52	0.09	**12.76**
9.94	15.04	15.08	20.28	15.06	21.13	5.12	14.37	10.07	**19.38**
19.99	24.02	24.92	31.09	24.97	31.86	14.99	21.82	19.86	**29.05**
30.01	35.99	35.03	44.57	34.97	44.9	24.97	32.58	30.15	**42.81**

5. Predictive thermodynamic method for assessing partial decomposition processes

The purpose of the procedure described in this section is to approximately quantify the contribution of undecomposed and decomposed portions of fluid on the determination of the saturation pressure of the system. A simplified thermodynamic analysis is applied to estimate the total molar fraction and saturation pressure of components generated from the partial decomposition of C_6F_{14} observed at 400°C. The analysis is applied to the saturation pressure data obtained from the partially decomposed fluid when subjected to vapour-liquid equilibrium (VLE) conditions.

When partial decomposition occurs, it can be assumed that C_6F_{14} is the prevalent component. Products generated by its decomposition are unknown and they likely change both in terms of chemical species and composition after each thermal stress. Due to the difficulty of precisely describing the chemical reactions involved during decomposition, here it is assumed that two main species are present in

the partially decomposed system: C_6F_{14} (indexed with i=1) and decomposition products (grouped in a "pseudo – comp. 2", indexed with i=2). Assuming the two phases being ideal mixtures of ideal gases and condensed components, it can be written, for each i-th component,

$$y_i P = x_i P_{sat,i} \text{ with i } = 1,2 \tag{2}$$

Thus, adding the contribution of the two species, where $y_1 + y_2 = 1$ and $x_1 + x_2 = 1$, it is obtained the total pressure of the system:

$$p = x_1 p_{sat,1} + (1 - x_1) p_{sat,2} \tag{3}$$

Finally, substituting in (3) the expression for x_1 resulting from (2), at saturation conditions (T_i, p^{T_i}),

$$p^{T_i} = \left(y_1 \tilde{p}_{sat,1}^{-1}(T_i) + (1 - y_1) p_{sat,2}^{-1}\right)^{-1} \tag{4}$$

It is now described how to apply Eq. (4) in order to determine the saturation pressure profile of "pseudo - component 2", $p_{sat,2}$, and the composition of the vapour phase, $\bar{y}$, considering that, for a generic saturation temperature T_i: (i) p^{T_i} in (4) is the saturation pressure of the fluid measured at temperature T_i after the thermal stress test; (ii) saturation pressure $\tilde{p}_{sat,1}(T_i)$ in (4) is determined through the Antoine equation initially calibrated over virgin fluid data (see Table 2). Moreover, in order to enable the computation of $\tilde{p}(T_i)$, the actual saturation pressure of the system after partial decomposition occurred at 400°C, for any arbitrary temperature T_i, the Antoine equation can be calibrated over saturation pressure measurements carried on after thermal stress at 400°C (see data in Table 3a). This modelling work is similar to the one performed with the saturation pressures of virgin fluid (see par. 3). In the analysis described in the followings, parameters of this calibrated model are indicated with A_{400} , B_{400}, C_{400}.

First we subdivide in K small intervals the temperature range where saturation pressure has been measured after the thermal stress test at T_s=400°C (i.e. ΔT=4°C with T= -19.92–30.15 °C, see Table 3b) and we further discretize each of these intervals into NP points (i.e. NP = 20). Then, for each of these points (i-th point at temperature T_i), we calculate the reference pressure $\tilde{p}_{sat,1}(T_i)$ and the actual saturation pressure $\tilde{p}(T_i)$ of the system after partial decomposition, through the relative calibrated Antoine equations: $p_{sat,1}(T_i) = A_0 - B_0/(C_0 + T_i)$ and $p(T_i) = A_{400} - B_{400}/(C_{400} + T_i)$. Finally, we minimize the following objective function, in each k-th temperature range ΔT, by regressing $p_{sat,2}$ and y_1:

$$\sum_{i=1}^{NP_{\Delta T_k}} \left(p(T_i) - \left(y_1 p_{sat,1}^{-1}(T_i) + (1 - y_1) p_{sat,2}^{-1}\right)^{-1}\right)^2 \tag{5}$$

The procedure described above has led to the representation of Figures 2 and 3. Figure 2 shows all the regressed values of vapour molar fraction of pseudo-component 2, y_2, and its saturation pressures in the temperature range -20–30°C. Moreover, Figure 3 shows saturation pressures of: (1) C_6F_{14} partially decomposed at T_s = 400°C [p]; (2) virgin C_6F_{14} [$p_{sat,1}$]; (3) decomposition components produced at 400°C, "pseudo-component 2" [$p_{sat,2}$]; (4) pure C_5F_{12} [$p_{sat,1}$]. With reference to Figure 3, the comparison between $p_{sat,1}$ and $p_{T_s=400°C}$ highlights the effect of the decomposition occurred at T_s = 400°C: the measured saturation pressure, $p_{T_s=400°C}$, is higher than $p_{sat,1}$ in the whole considered temperature range. The reason of this pressure change lies probably in the production of lighter unsaturated molecules of free radicals which combine to form polymers [3, 17]. Moreover, the presence of air, deriving from an incomplete degassing, would justify the formation of CO and CO_2, as detected by [18, 7]. Figure 3 also shows that, at temperature lower than 15°C, saturation pressure of decomposition products, $p_{sat,2}$, is similar to the one of C_5F_{12}. This remark indicates that decomposition products could be mainly composed of C_5F_{12}. Moreover, the deviation of $p_{sat,2}$ from pure C_5F_{12} with temperature would demonstrate the presence of lighter gases which tend to increase the saturation pressure of the system as the temperature increases. This result confirms some conclusions achieved by [18, 7]: (1) fluorocarbons start their thermal decomposition with the rupture of C-C bonds rather than C-F ones, giving rise to lighter fluorocarbons; (2) low temperature thermal

decompositions mainly lead to the rupture of "external" C-C bonds of C_6F_{14}, producing radicals such as -CF_3 and -C_5F_{11}.

It is worth noting that studies carried out by [19,20] on vapour-liquid equilibrium binary systems containing fluorocarbons of similar size, such as cyclo-C_5F_{10} – n-C_5F_{12} and cyclo-C_5F_{10} – n-C_6F_{14}, have proved their ideality. Thus, the initial assumption of ideal system, which the analysis has been based on, is reasonable.

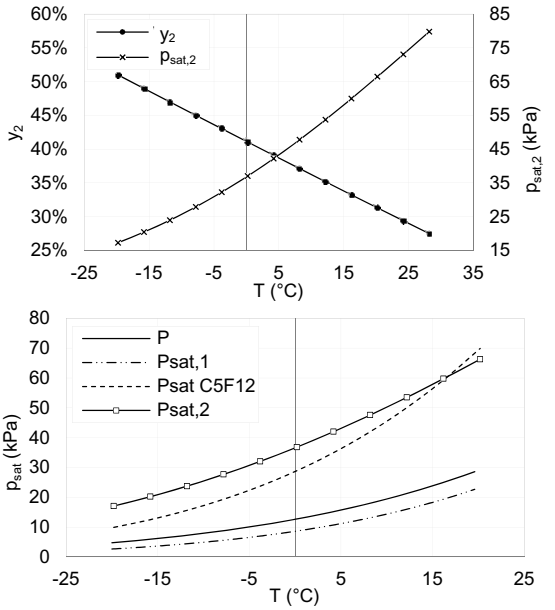

Fig. 2. Characteristics of pseudo-component 2: regressed values of vapour molar fraction of "pseudo-comp.2" generated at T_s = 400°C [y_2], and its saturation pressures [$P_{sat,2}$].

Fig. 3. (1) Saturation pressure profiles of C_6F_{14} partially decomposed at T_s = 400°C [P]; (2) virgin C_6F_{14} [$P_{sat,1}$]; (3) "pseudo-comp. 2" generated at T_s = 400°C [$P_{sat,2}$]; (4) virgin C_5F_{12} [$P_{sat,C5F12}$].

6. Conclusions

In this paper we report the experimental results of the thermal stability of Perfluorohexane (C_6F_{14}) in view of its potential use in mixture with CO_2 as an innovative working fluids for Organic Rankine Cycles.

Results of the analysis prove that pure Perfluorohexane can be considered stable up to 350 °C, showing early signs of decomposition after the thermal stress test at 400 °C. Moreover, the development of a theoretical predictive decomposition model applied to the partially decomposed system has enabled the detection of reactions that entail the rupture of C-C bonds and the production of -CF_3 and -C_5F_{11} radicals.

In future works, the experimental analysis of thermal stability of the CO_2-C_6F_{14} mixture will be carried out, as well as the evaluation of performances of a transcritical power cycle that employs such mixture as working fluid, in order to provide indications on its potential application.

References

[1] Chen Y. *Thermodynamic Cycles using Carbon Dioxide as Working Fluid. CO_2 Transcritical power cycle study*. Doctoral thesis. School of Industrial Engineering and Management. Stockholm, 2011

[2] Colina CM, Galindo A, Blas FJ, Gubbins KE. Phase behavior of carbon dioxide mixtures with n-alkanes and n-perfluoroalkanes. *Fluid Phase Equilib.* 2004; **222–223**: 77–85.

[3] Lemal DM. Perspective on Fluorocarbon Chemistry. *J. Org. Chem.* 2004; **69**: 1-11.

[4] Dardin A, DeSimone JM, Samulski ET. Fluorocarbons Dissolved in Supercritical Carbon Dioxide. NMR Evidence for Specific

Solute-Solvent Interactions. *J. Phys. Chem. B* 1998; **102**: 1775-80.

[5] Lazzaroni MJ, Bush D, Brown JS, and Eckert CA. High-Pressure Vapor-Liquid Equilbria of Some Carbon Dioxide + Organic Binary Systems. *J. Chem. Eng. Data*. 2005; **50**: 60-65

[6] Pachauri RK, Reisinger A. *Fourth Assessment Report of the Intergovernmental Panel on Climate Change*. IPCC, Geneva, Switzerland, 2007

[7] Arnold WA, Hartman TG, McQuillen J. Chemical Characterization and Thermal Stressing Studies of Perfluorohexane Fluids for Space-Based Applications. NASA - Glenn Research Center, 2006.

[8] Pasetti M, Invernizzi CM, Iora P. Thermal stability of working fluids for organic Rankine cycles An improved survey method and experimental results for cyclopentane, isopentane and n-butane. *Appl. Therm. Eng.* 2014; **73**: 762-72.

[9] Stiles VE, Cady GH. Physical properties of perfluoro-n-hexane and perfluoro-2-methylpentane. *J. Am. Chem. Soc*. 1952; **74**: 3771-73.

[10] Dunlap RD, Murphy CJ, Bedford RG, Young JA. Some physical properties of perfluoro-n-hexane. *J. Am. Chem. Soc*. 1958; **80**: 83-5

[11] Crowder GA, Taylor ZL, Reed TM. Young JA. Vapor Pressures and Triple Point Temperatures for Several Pure Fluorocarbons.. *Chem. Eng. Data*, 1967; **12**:481-5

[12] Mousa AHN. Study of Vapor Pressure and Critical Properties of Perfluoro-n-Hexane. *J. Chem. Eng. Data*, 1978; **23**: 133-4

[13] Dias AMA, Goncalves CMB, Caco AI, Santos LM, Pineiro MM, Vega L, Coutinho JAP, Marrucho IM. Densities and Vapor Pressures of Highly Fluorinated Compounds. *J. Chem. Eng. Data*, 2005; **50**: 1328-33.

[14] Wagner W. *A new correlation method for thermodynamic data applied to the vapour pressures of argon, nitrogen and water*. I.U.P.A.C. Thermodynamic Tables Project Centre: Imperial College. London; 1977

[15] Ambrose D, Ghiassee NB. Vapour pressures and critical temperatures and critical pressures of C_5 and C_6 cyclic alcohols and ketones. *J. Chem. Thermodynamics* 1987; **19**: 903-909.

[16] Antoine C. Tensions des vapeurs, nouvelle relation entre les tensions et les températures. *CR ACAD SCI II C*, 1888; **107**: 681-84, 778-80, 836-37

[17] Steunenberg RK, Cady GH. Pyrolysis of Fluorocarbons. *J. Am. Chem. Soc*. 1952; 74; 4165-68

[18] Hynes RG, Mackie JC, Masri AR. Shock-Tube Study of the Pyrolysis of the Halon Replacement Molecule CF_3CHFCF_3. *J. Phys. Chem. A* 1999, 103, 54-61

[19] Scott RL. The anomalous behavior of fluorocarbon solutions. *J. Phys. Chem*., 1958; **62**: 136–145

[20] Newcome MM, Cady GH. Liquid-Vapor Equilibria in Fluorocarbon Systems. *J. Am. Chem. Soc*., 1956; **78**: 5216-5218

Biography of the corresponding author

Doctoral student in "Energy and Nuclear Science and Technology" since 2012 at *Politecnico di Milano*, Miss. Lasala performes experimental and modelling activities aimed at describing the thermodynamics and stability characteristics of CO_2-based mixtures relevant for energy conversion applications: CO_2-capture and storage, refrigeration cycles, supercritical-CO_2 and organic Rankine power cycles.